MOLECULAR AND CELLULAR BIOLOGY, Nov. 2011, p. 4430–4441 Vol. 31, No. 22
0270-7306/11/$12.00 doi:10.1128/MCB.05474-11

The Aarskog-Scott Syndrome Protein Fgd1 Regulates Podosome Formation and Extracellular Matrix Remodeling in Transforming Growth Factor β-Stimulated Aortic Endothelial Cells▽

Thomas Daubon,[1,2,3] Roberto Buccione,[4]* and Elisabeth Génot[1,2,3,5]*

Université de Bordeaux, Physiopathologie du Cancer du Foie, U1053, F-33000 Bordeaux, France[1]; INSERM, Physiopathologie du Cancer du Foie, U1053, F-33000 Bordeaux, France[2]; European Institute of Chemistry and Biology, 2 Rue Robert Escarpit, 33 607 Pessac, France[3]; Tumor Cell Invasion Laboratory, Consorzio Mario Negri Sud, S. Maria Imbaro, Chieti 66030, Italy[4]; and CHU de Bordeaux, F-33076 Bordeaux, France[5]

Received 8 April 2011/Returned for modification 10 May 2011/Accepted 31 August 2011

Podosomes are dynamic actin-rich adhesion plasma membrane microdomains endowed with extracellular matrix-degrading activities. In aortic endothelial cells, podosomes are induced by transforming growth factor β (TGF-β), but how this occurs is largely unknown. It is thought that, in endothelial cells, podosomes play a role in vessel remodeling and/or in breaching anatomical barriers. We demonstrate here that, in bovine aortic endothelial cells, that the Cdc42-specific guanine exchange factor (GEF) Fgd1 is expressed and regulated by TGF-β to induce Cdc42-dependent podosome assembly. Within 15 min of TGF-β stimulation, Fgd1, but none of the other tested Cdc42 GEFs, undergoes tyrosine phosphorylation, associates with Cdc42, and translocates to the subcortical cytoskeleton via a cortactin-dependent mechanism. Small interfering RNA-mediated Fgd1 knockdown inhibits TGF-β-induced Cdc42 activation. Fgd1 depletion also reduces podosome formation and associated matrix degradation and these defects are rescued by reexpression of Fgd1. Although overexpression of Fgd1 does not promote podosome formation *per se*, it enhances TGF-β-induced matrix degradation. Our results identify Fgd1 as a TGF-β-regulated GEF and, as such, the first GEF to be involved in the process of cytokine-induced podosome formation. Our findings reveal the involvement of Fgd1 in endothelial cell biology and open up new avenues to study its role in vascular pathophysiology.

The cytokine transforming growth factor β (TGF-β) induces pleiotropic effects. It is a pivotal regulator of vascular homeostasis, in particular in the arterial tree, during adult life (15), but how it fulfils this particular role remains unclear. We recently uncovered a novel role for TGF-β in endothelial cell physiology. In the cultured bovine aortic endothelial (BAE) cell model, TGF-β was found to remodel the actin cytoskeleton giving rise to the formation of podosomes. These typically occur in large, ring-shaped clusters of about 8 μm in diameter (podosome superstructures also termed rosettes) (32). Podosomes are specialized plasma membrane actin-based microdomains consisting of a core of actin filaments associated with the Arp-2/3 based actin polymerization machinery and surrounded by a ring of focal adhesion proteins. They can be distinguished from typical focal adhesions complexes by the presence of gelsolin, cortactin, dynamin 2, and WASP/N-WASp proteins ("podosomal markers") (14, 19) and by the presence of metalloproteases such as MT1-MMP and MMP9. The latter endow podosomes with matrix degrading activities, as demonstrated by the multiple matrix "perforations" (round patches of degraded matrix) that occur underneath cells cultured on fluorophore-conjugated extracellular matrix proteins such as gelatin or collagen (32).

In the unchallenged blood vessel, the normal resting endothelium is devoid of podosomes (28). However, TGF-β stimulation of endothelial cells within cultured aortic vessel segments also leads to podosome formation and, again, this affects the underlying substratum, i.e., the vessel basement membrane (28). Endothelial podosomes may thus play an important role in vessel remodeling and/or in breaching anatomical barriers (29). Many studies have described the composition, organization, and function of these structures, but the initial events driving assembly of podosome components remain undefined. In smooth vascular cells where podosomes assemble in response to phorbol esters, the process is initiated by cortactin clustering near the ends of stress fibers that appear to act as nucleation platforms onto which the actin polymerization machinery assembles (34). Maturation of these prepodosomes occurs by subsequent translocation of additional cortactin to the F-actin cores and relies on cortactin actin-binding repeats and tyrosine phosphorylation which play a major role in actin dynamics at the structures. A better understanding of these initial events may help to define the cellular context in which endothelial podosomes come into play.

Actin cytoskeleton remodeling in response to extracellular cues is driven by members of the Rho GTPase family which includes Cdc42, Rho, and Rac (24). Previous studies have revealed a master role for Cdc42 in the process of podosome

* Corresponding author. Mailing address for Elisabeth Génot: European Institute of Chemistry and Biology, 2 Rue Robert Escarpit, 33 600 Pessac, France. Phone: 33 5 40 00 30 56. Fax: 33 5 40 00 87 26. E-mail: e.genot@iecb.u-bordeaux.fr. Mailing address for Roberto Buccione: Tumor Cell Invasion Laboratory, Consorzio Mario Negri Sud, Via Nazionale 8/A, S. Maria Imbaro, Chieti 66030, Italy. Phone: 39-0872-570353. Fax: 39-0872-570412. E-mail: buccione@negrisud.it.

▽ Published ahead of print on 12 September 2011.

formation downstream of Src family kinases (31) and in response to TGF-β (32). In aortic endothelial cells, a constitutively active form of Cdc42 is sufficient to allow the formation of podosomes, which, however, arise as individual entities scattered all over the ventral membrane (20, 21), instead of being organized in superstructures.

The Rho GTPases cycle between inactive GDP-bound and active GTP-bound states but have limited hydrolytic and exchange activity on their own and thus require accessory proteins to function efficiently and to ensure proper regulation. These are included in three classes: guanine nucleotide exchange factors (GEFs), GTPase-activating proteins and guanine nucleotide exchange inhibitors. The GEFs stimulate the exchange of GDP for GTP to generate the activated form and are much more numerous than the Rho GTPases themselves (30). Hence, although how GEFs are regulated is still unknown, they clearly represent powerful candidates as spatial and temporal Rho GTPase regulators by modulating the specificity of downstream signaling from Rho GTPases in diverse cellular functions and cell systems (38).

We sought to identify the GEF(s) responsible for TGF-β-induced Cdc42 activation in the process of endothelial podosome formation. Published reports hint to a number of possible candidates. Phorbol-ester-mediated podosome formation in vascular smooth muscle cells requires βPIX (ARHGEF9) (33). It serves as a dual function GEF/signaling-effector for Cdc42 also playing a role in cell transformation as a consequence of Src transformation (11). A related GEF, αPix (ARHGEF6) influences podosome formation and size (12), whereas Vav2 has been reported to play a role in angiogenesis (4). As for the TGF-β pathway, Zizimin1 (DOCK9) was found to associate with Smad2 and Smad3 proteins (5). Finally, and more recently, Fgd1 (3) was shown to be required for the formation of invadopodia, podosome-related structures commonly found in cancer cells (6), the formation of which also relies on Cdc42. Fgd1 is part of a family comprising seven members with significant homologies in the C-terminal portion of the molecule but major divergence in the N-terminal region (Fig. 1) (23). Of note, Frabin (Fgd4) was also shown to regulate invadopodia function (22). Here, we describe expression of Fgd1 in endothelial cells and show that it regulates TGF-β-mediated podosome formation as well as matrix degradation through direct activation of Cdc42. Fgd1 is already known as an important actor in skeletal formation because mutations in the gene result in the disease faciogenital dysplasia or Aarskog-Scott syndrome (AAS), characterized by short stature and facial, limb, and genital anomalies. The gene is located on the short arm of the X chromosome (Xp11.2), thus mutations in the Fgd1 gene produce full expression in males. Females with one mutated gene allele may have subtle facial differences and less height than other females in the family. However, there is evidence that an autosomal dominant or recessive form also exists. Both autosomal dominant and recessive patterns of inheritance remain possible (35). Missense and nonsense deletions and insertions are reported in addition to gross rearrangements. No mutational hot spots or common mutations are seen and no evident genotype-phenotype correlation is apparent from comparison of patients with different mutations. There is, to date, no mouse model for the disease. This study on Fgd1 regulation in endothelial cell biology points at a possible role for Fgd1 in vascular diseases.

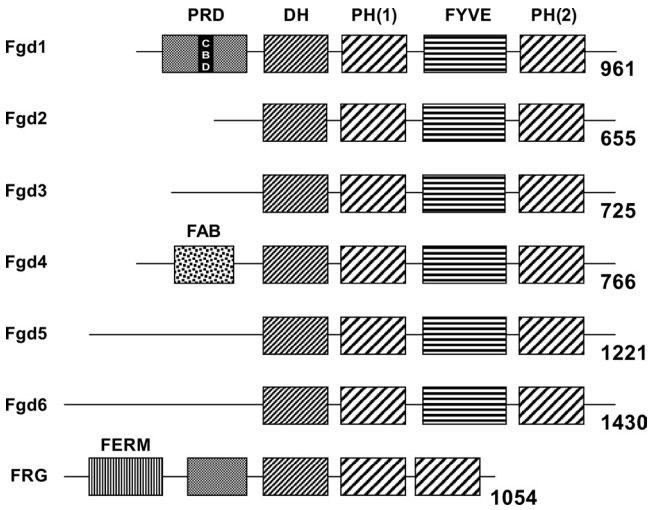

FIG. 1. Fgd family. Fgd1 is the founding member of a family of seven related Fgd1-like genes encoding modular proteins containing in sequence an N-terminal domain, a Dbl homology (DH) domain, an adjacent plekstrin homology (PH1) domain, a FYVE-finger domain (with the exception of FRG [Fgd1-related GEF]), and a second C-term PH domain (PH2). The N-terminal domain is highly variable and contains a cortactin/Mabp1 binding domain (CBD) within a proline-rich domain (PRD) in Fgd1, an actin-binding domain (FAB) in Fgd4 (Frabin) and a FERM domain in FRG. Numbers refer to amino acid residues.

MATERIALS AND METHODS

Cells. BAE cells (Lonza) were maintained in complete endothelial cell growth medium (EGM-MV; Promocell) at 37°C in a 5% CO_2 humidified atmosphere and used between passages 2 and 7.

Reagents. Recombinant human TGF-β1 (used at 5 ng/ml in all experiments) was obtained from R&D Systems. Glutathione-Sepharose beads, PP2 and SU6566, and antibodies against vinculin (hVIN-1), tubulin and Fgd1 (Ab#1) were purchased from Sigma. Our Fgd1 antiserum (Ab#2) was described previously (3). Other antibodies against the following proteins were obtained as follows: cortactin (clone 4F11), N-WASp, P-Smad2/3, and phosphotyrosine antibodies (4G10Platinum; Millipore); anti-myc (9E10), MT1-MMP, and Vav2 (Abcam); Smad1 and CD31 (Santa Cruz); P(416)-Src (Invitrogen); Cdc42, αPIX, βPIX, and P-Smad1/5/8 (Cell Signaling Technology); Smad2/3 (BD Biosciences); and green fluorescent protein (GFP; Roche). Cdc42-GTP conformation-specific antibodies were from NewEast Biosciences. Alexa 546-phalloidin-, Alexa 488-, or Alexa 647-labeled secondary antibodies, and Hoechst 33342 were purchased from Molecular Probes.

Immunofluorescence staining. Subconfluent cells grown on glass coverslips were fixed with 3.7% paraformaldehyde prepared in cytoskeletal buffer (32). The coverslips were washed in water and mounted on microscope slides with Fluoromount mounting medium (Clinisciences). Immunostaining for the detection of active Cdc42 was performed after an additional blocking step with iT reagent (Invitrogen) and prolonged incubation with the conformational anti-Cdc42-GTP antibodies. The coverslips were mounted with antifade reagent (Invitrogen).

Microscopy and image analysis. Cells were analyzed by confocal imaging using a Zeiss LSM 510 Meta inverted laser scanning fluorescence microscope equipped with acquisition software (LSM 510 acquisition software; Zeiss) and a ×63 (numerical aperture [NA], 1.4) oil immersion objective. Triple- or quadruple color imaging using Hoechst 33342-labeled, Alexa 488-labeled, and/or Alexa 647-labeled secondary antibodies or Alexa 546-phalloidin was obtained using selective laser excitation at 350, 488, and 647 nm or at 543 nm, respectively. Each channel was imaged sequentially using the multitrack recording module before merging. Fluorescent images were processed with Adobe Photoshop 7.0. Quantification of cells showing podosome rosettes was done by counting at least 500 cells for each coverslip.

Western blotting. Cells were collected in reducing Laemmli sample buffer, and then the samples were boiled and subjected to sodium dodecyl sulfate-polyacrylamide gel electrophoresis. Proteins were transferred from gels to Immobilon polyvinylidene difluoride membranes (Millipore). Proteins were detected by chemiluminescence (GE Healthcare) using horseradish peroxidase-coupled secondary antibodies (Dako). In some experiments, the amounts of proteins detected by Western blotting were determined by scanning the autoradiograph, followed by processing of the data with NIH Image software.

Cdc42 activity assay. Cdc42 total activities were measured by pulldown assays using glutathione *S*-transferase (GST)–Cdc42-interactive binding domain (CRIB)–N-WASp (32). Cdc42 activity was quantified as the ratio of the measured staining intensity of the GTP-Cdc42 band pulled down with GST-N-WASp divided by that measured for tubulin, which was used to normalize protein loading.

Fractionation protocol. Cells were treated with TGF-β for various times, washed, and lysed in 5 mM Tris-HCl (pH 7.5), mM NaCl, 1 mM $CaCl_2$, 1 mM $MgCl_2$, 2 mM dithiothreitol, 1 mM Na_3VO_4, 10 mM NaF, 0.1 mM phenylmethylsulfonyl fluoride, and protease inhibitors for 30 min on ice. Samples were then centrifuged at 100,000 × *g* (1 h, 4°C). Pellets (membrane/cytoskeletal fractions) were solubilized in 1% Triton-containing buffer and run in parallel with supernatants (cytosol).

Immunoprecipitation. Cells were washed with ice-cold serum-free medium and lysed on ice in buffer containing 20 mM Tris-HCl (pH 7.4), 150 mM NaCl, 1 mM EGTA (pH 8.0), 1 mM EDTA (pH 8.0), 2.5 mM pyrophosphate, 1 mM β-glycerophosphate, 1% Triton X-100 containing freshly added protease, and phosphatase inhibitor cocktail tablets (Roche). Lysates were clarified by centrifugation at 4°C, and the protein concentrations were determined by using Bio-Rad protein assay reagent (Bio-Rad Laboratories). For immunoprecipitation analyzes, aliquots of cellular lysates were incubated with 2 μg of polyclonal anticortactin, antiphosphotyrosine, or anti-GFP antibodies for 1 h at 4°C. Immunocomplexes were collected on protein G-Sepharose beads (Sigma). The beads were washed three times with lysis buffer then boiled for 3 min in Laemmli sample buffer.

siRNA and transfection. Small interfering RNA (siRNA; Qiagen) transfection into BAE cells was performed by two rounds of transfection with double-stranded RNA (50 nM) (32). On the next day, cells were stimulated with TGF-β for the indicated times and analyzed. The RNA target sequences siRNA Fgd1**#**1 (AAGTCTCTGGAGCTGATAGCC), siRNA Fgd1**#**2 (AACCTCAATCTGCC TCGGACC), siRNA Fgd1**#**3 (AAGAGGTGCCAGTGGCAGCTT), and siRNA cortactin (AAGCACTGCTCGCAGGTTGAC) were designed against the corresponding bovine cDNA using online algorithms (Dharmacon and/or Applied Biosystems). AllStars Negative Control siRNA (Qiagen) was used as a control in all siRNA gene-silencing experiments. Fluorescence-activated cell sorting experiments using Alexa 488-siRNA (Qiagen) showed 95 to 98% transfection efficiency.

Expression constructs and transfection. The Cdc42G15A construct was kindly provided by Keith Burridge (University of North Carolina, Chapel Hill). GFP-Fgd1 contains the nearly full-length Fgd1 cDNA (amino acid residues 18 to 960) fused to an in-frame 5′GFP epitope tag. The myc-Fgd1-RKB3 fusion construct contains deletions of residues 1 to 391 and 790 at the C terminus (25, 38). The GFP-Fgd1-2DBDEL fusion construct contains deletions of residues 146 to 188 and 730 at the C terminus (3, 9). All Fgd1 encoding plasmids were obtained from J. L. Gorski (University of Michigan) (3). Cells were transfected using nucleofector technology (Neon; Invitrogen) according to the manufacturer's guidelines (4 μg for a 35-mm dish) and, 24 h after transfection, the cells were stimulated with TGF-β for the indicated times and analyzed.

Matrix degradation assay. BAE cells were seeded on fluorescein isothiocyanate (FITC)-gelatin-coated coverslips (32). Quantification of degradation areas on FITC-labeled gelatin was performed for at least 20 fields (×10 objective lens) for each coverslip. The areas of degradation were quantified by using ImageJ software, and the total degradation area (expressed in mm^2) was then normalized for the number of cells (at least 300 cells were counted). Control values were arbitrarily taken as 100%.

Statistics. Each experiment was performed at least three times, and quantification values represent the means of three independent experiments ± the standard deviations. The significance was determined by using a Student *t* test, and *P* values of <0.05 were considered statistically significant.

RESULTS

Fgd1 is expressed in aortic endothelial cells and is regulated by TGF-β. To identify the activator of Cdc42 downstream of TGF-β-mediated signaling, we took advantage of the nucleotide-free Cdc42 mutant Cdc42G15A, which has a high affinity for activated Cdc42-GEFs (8, 13). BAE cells were left untreated or treated with TGF-β for 30 min and lysed, and pulldowns were performed with purified GST-Cdc42G15A proteins. Upon Western blotting, a protein band was revealed with anti-Fgd1 antibodies (Ab**#**1) but not with antibodies recognizing other Cdc42 GEFs such as αPIX, βPIX, Vav2, or Zizimin (Fig. 2A). Since Fgd1 is predominantly expressed in osteoblasts and has not been described in endothelial cells, we sought to confirm its expression in BAE cells. First, the presence of Fgd1 transcripts was verified by quantitative real-time PCR (data not shown). To verify the presence of Fgd1 protein, after Western blotting, both commercial antibodies (Ab**#**1) and anti-Fgd1 immune serum raised in rabbits (Ab**#**2) (3) were tested. Both antibodies labeled proteins of similar molecular masses and corresponding to the predicted size of Fgd1 (107 kDa) in whole-cell lysates prepared from BAE cells (endogenous protein), as well as in BAE cells transfected with a GFP-Fgd1 encoding construct (130 kDa) (Fig. 2B and Fig. 3),

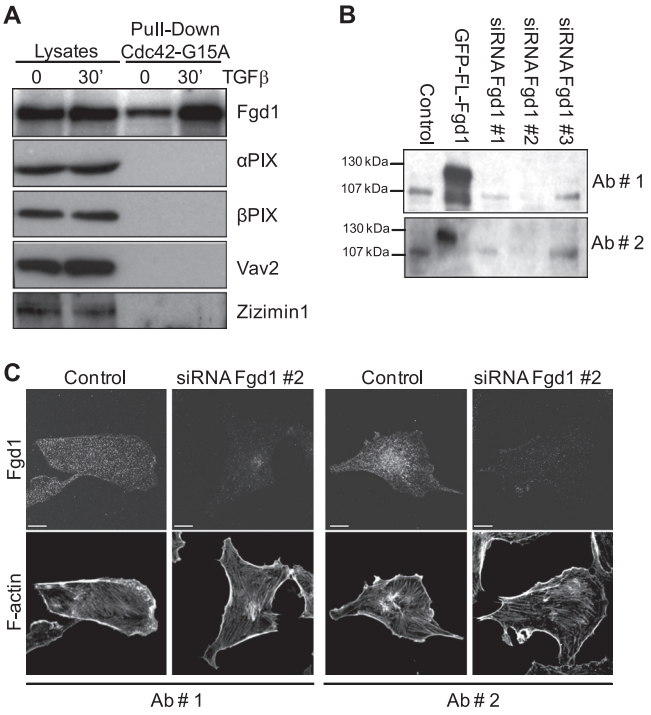

FIG. 2. Fgd1 is expressed in aortic endothelial cells. (A) Cells were stimulated or not with 5 ng of TGF-β/ml for 30 min, lysed, and subjected to the pulldown assay using a Cdc42G15A-GST fusion protein. The samples and a fraction of the corresponding lysate were then analyzed by Western blotting with anti-Fgd1 (Ab#1), anti-αPIX, anti-βPIX, anti-Vav2, or anti-Zizimin1 antibodies. (B) Cells were independently transfected with different siRNAs (#1 to #3) targeting Fgd1 and then transfected with GFP or GFP-FL-Fgd1 encoding constructs. On the next day, cell lysates were prepared and analyzed by Western blotting, using either commercial anti-Fgd1 antibodies (Ab#1) or homemade anti-Fgd1 antibodies (Ab#2). (C) Fgd1 protein expression was inhibited using siRNA Fgd1 #2, and TGF-β stimulation was performed 24 h after the second siRNA transfection. Immunostainings for Fgd1 were performed with anti-Fgd1 antibody (Ab#1 or Ab#2) revealed with Alexa 488 secondary antibodies, together with phalloidin-Alexa 546 and Hoechst. Bar, 10 μm.

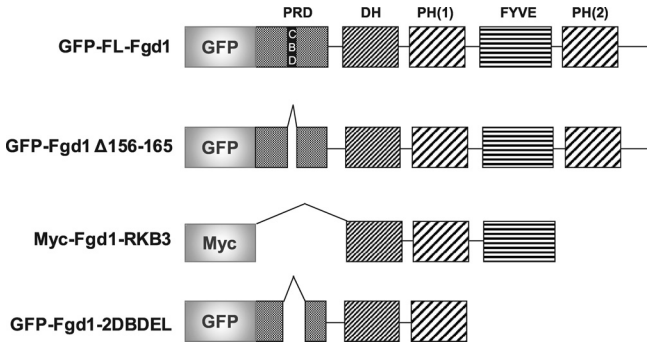

FIG. 3. Plasmids used in the present study. A schematic diagram of the Fgd1 encoding vectors used in this study is shown.

as revealed after probing the blots with anti-GFP antibodies (data not shown). The intensity of the bands revealed with either antibody appeared decreased when siRNAs designed to target bovine Fgd1 were transfected, with the strongest effect seen with siRNA#2 (Fig. 2B). Fgd1 was also detected by immunofluorescence in individual cells. Staining with either antibody revealed that Fgd1 mainly localizes in the cytosol. A very small fraction of the protein was detected at the cell cortex when Ab#2 was used, indicating that this antibody was more sensitive than Ab#1 (Fig. 2C). Fgd1 staining was greatly reduced in cells transfected with siRNA#2 (Fig. 2C). Fgd1 was thought to be mainly expressed in osteoblasts and derived cell lines (16, 18) and was more recently shown to be expressed in certain tumor-derived cell lines and human tumors (3). These results conclusively demonstrate that Fgd1 is also expressed in primary endothelial cells.

TGF-β activates Fgd1 in aortic endothelial cells. Data presented in Fig. 2A indicated that the amount of Fgd1 pulled down with Cdc42G15A increased upon TGF-β stimulation. How GEFs are regulated is still unclear, but there are indications that many Rho-family GEFs are regulated by tyrosine phosphorylation (36). We thus investigated if Fgd1 was phosphorylated and if so, whether it was affected by TGF-β. To this end, Fgd1 tyrosine phosphorylation was examined in the Cdc42G15A pull down from samples prepared from cells treated with TGF-β for increasing time periods (Fig. 4A). Western blot experiments performed with anti-Fgd1 antibodies revealed a band corresponding to the molecular weight of Fgd1, whose intensity increased within the first hour of exposure, peaked between 1 and 4 h and decreased upon prolonged incubation with TGF-β (Fig. 4A). Similar results were obtained when 4G10 anti-phosphotyrosine antibodies were used to reveal Cdc42G15A bound proteins from a parallel experiment, although the increase in protein phosphorylation appeared to precede that of Fgd1 binding to Cdc42G15A (Fig. 4A). These results suggested but did not prove that Fgd1 was phosphorylated upon TGF-β stimulation. The affinity precipitation assay for activated GEF was therefore performed with Fgd1-depleted BAE cells. The band corresponding to Fgd1 and the phosphorylated band at the corresponding molecular mass were no longer detected after silencing Fgd1 expression (Fig. 4B). Next, the converse experiment was performed by immunoprecipitating anti-tyrosine-phosphorylated protein and probing the samples with anti-Fgd1 antibodies. A weak basal

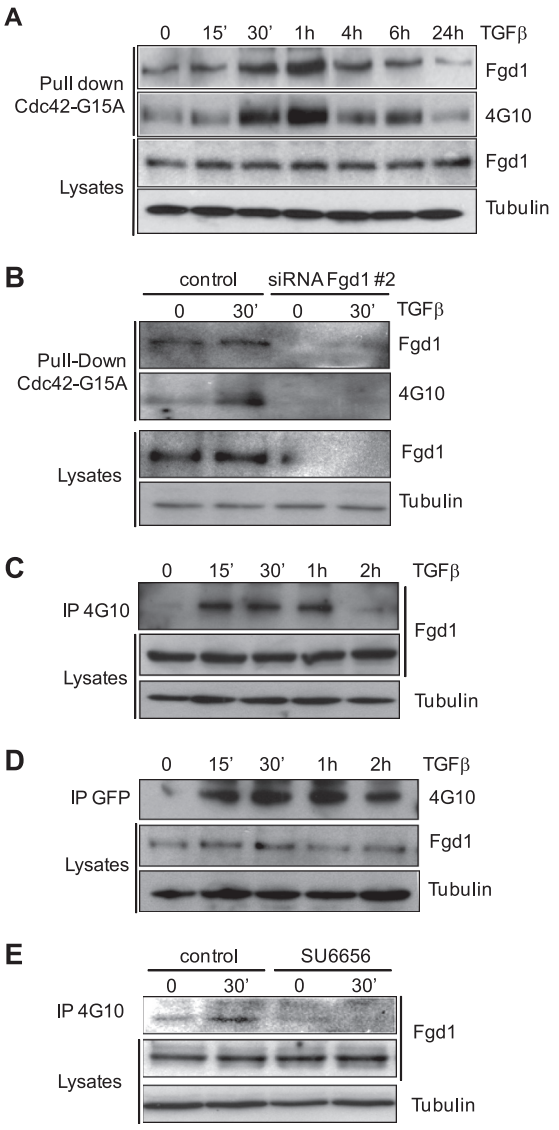

FIG. 4. Fgd1 is activated in response to TGF-β. (A) BAE cells stimulated with TGF-β for different time periods were subjected to a Cdc42G15A-GST pulldown assay, and the membranes were incubated with either anti-Fgd1 (Ab#1) or antiphosphotyrosine (4G10) antibodies. Similar Fgd1 and tubulin levels seen in all lanes of corresponding lysates demonstrate equal protein loading. (B) Fgd1 was knocked down in BAE cells, and a 30-min TGF-β stimulation was performed 24 h after the second siRNA transfection. A pulldown assay was then performed as in panel A. (C) BAE cells were stimulated with TGF-β for different time periods, and phosphoproteins were immunoprecipitated with 4G10 antibodies. Immunoprecipitated proteins were analyzed for Fgd1 content (Ab#1). Similar Fgd1 and tubulin levels seen in all lanes corresponding to cell lysates demonstrate equal protein loading. (D) BAE cells were transfected with GFP-FL-Fgd1 and, on the next day, stimulated with TGF-β for increased periods of time. GFP fusion proteins were immunoprecipitated with GFP antibodies and analyzed for phosphorylation (4G10) and Fgd1 content (Ab#1). Similar GFP-Fgd1 and tubulin levels seen in all lanes corresponding to cell lysates demonstrate equal protein loading. (E) BAE cells were treated for 1 h with 10 μM SU6656 and then stimulated with TGF-β for 30 min, and phosphoproteins were immunoprecipitated and analyzed as in panel C.

Fgd1 phosphorylation was observed in untreated cells whose intensity was enhanced upon 15 min of TGF-β treatment; the signal peaked at around 30 min and decreased thereafter (Fig. 4C). Similar results were obtained when the immunoprecipitation was performed with anti-GFP antibodies from cells which had been transfected with GFP-tagged FL-Fgd1 (Fig. 4D). Previously published data obtained in this model showed Src regulation upon exposure to TGF-β (32). We therefore examined the consequences of Src inhibition on this response. The data presented in Fig. 4E show that SU6656 (or PP2 [data not shown]) completely abolished Fgd1 phosphorylation. Collectively, these results indicate that, upon TGF-β stimulation, Fgd1 is first tyrosine phosphorylated in a Src-dependent manner and thereafter associates with Cdc42 and that such association is maintained during the first hours of TGF-β stimulation.

Fgd1 is required for podosome formation through Cdc42 activation. To directly explore the involvement of Fgd1 in the TGF-β signaling cascades leading to podosome formation, Fgd1 expression was silenced with the independent siRNA duplexes presented in Fig. 2B. Fgd1-depleted cells exhibited subtle alterations in cytoskeleton organization with slightly more prominent cortical F-actin in a minority of cells. When exposed to TGF-β, Fgd1 silenced cells exhibited much fewer podosome rosettes than control cells (Fig. 5A). The decrease in the number of podosome-forming cells was inversely proportional to the amount of remaining Fgd1, with siRNA#2 giving the strongest effect (Fig. 5A and B). In these conditions, cells did not efficiently degrade the matrix (Fig. 5A). Reexpression of Fgd1 by transfecting GFP-tagged murine Fgd1 rescued podosome formation (Fig. 5C to E). The consequences of Fgd1 depletion on Cdc42 activity in TGF-β-treated cells were monitored by a pulldown assay using a fusion protein containing the Cdc42 interacting domain of N-WASp. Fgd1 silencing did not affect basal GTP-Cdc42 levels measured in untreated cells but reduced Cdc42 activation 2-fold at the peak of the response (32) (Fig. 5F and G). Thus, Fgd1 is required for TGF-β-mediated Cdc42 activation and podosome formation.

Fgd1 translocates to cell membranes upon TGF-β stimulation. The activation of RhoGEFs is known to be intimately coupled with their targeting to appropriate cellular destinations. We therefore examined whether Fgd1 redistribution occurred upon TGF-β stimulation. In untreated BAE cells, Fgd1 staining appeared cytoplasmic, enriched in the perinuclear region and with only a very minor pool of the protein being sporadically visible at plasma membrane protrusions (Fig. 6A). Upon TGF-β treatment, Fgd1 staining increased at the cell cortex as early as 15 min and persisted for 1 h. Fgd1 redistribution occurred concomitantly with its phosphorylation (Fig. 6A). In most cells, prominent staining was seen at cell protrusions. The spatiotemporal activation of Cdc42 was examined in parallel using a configuration-specific monoclonal antibody that recognizes Cdc42-GTP but not Cdc42-GDP. A weak perinuclear staining was seen in untreated cells. At all time points of the TGF-β stimulation period, Cdc42-GTP staining was found enhanced compared to control cells, and colocalization between Fgd1 and Cdc42-GTP was observed at early time points after the TGF-β addition (15 to 60 min) (Fig. 6A), consistent with a possible interaction of the two proteins. Fgd1 binds cortactin through its proline rich N-terminal domain (Fig. 3), and this region has been shown to be necessary and sufficient for Fgd1 subcellular localization at the membrane (16). The subcellular distribution of cortactin was therefore examined in parallel. In untreated cells, cortactin was mainly cytosolic but also detected at cell protrusions. Upon TGF-β stimulation, cortactin staining rapidly increased at the cell cortex, with kinetics similar to those observed for Fgd1 (Fig. 6A). Colocalization of Fgd1 and cortactin was observed at early time points following TGF-β addition (15 to 60 min), indicating that Fgd1, Cdc42-GTP, and cortactin all colocalized during this period. Fgd1 was still found localized at actin rings in ca. 20% of podosome rosettes at 24 h (Fig. 6A). Similar results were seen in cells expressing the GFP-FL-Fgd1 construct (data not shown). This fusion protein showed the same localization pattern as those previously shown in other cell types (10) but, in contrast to the situations encountered in other cell types (10, 23), did not induce filopodia in BAE cells. Upon TGF-β stimulation, the relocalization of GFP-FL-Fgd1 was similar to that of the endogenous protein (data not shown). We next examined the subcellular localization of Fgd1 by performing subcellular fractionation, as an alternative approach to demonstrate Fgd1 translocation to membranes. Consistent with the immunofluorescence data, Fgd1 was found in the cytosolic fraction with a minor amount sedimenting with the plasma membrane/cytoskeletal fraction (Fig. 6B). After 15 min of TGF-β stimulation, the amount of Fgd1 found in the insoluble fraction was dramatically increased, reflecting Fgd1 translocation to plasma membrane/cytoskeleton compartments. Interestingly, cortactin was found to undergo membrane translocation with a strikingly similar pattern (Fig. 6B). Although it is known that the two protein associate, whether this association is regulated has not been investigated. Cells were treated with TGF-β and cortactin was immunoprecipitated at various time points after TGF-β addition. Western blotting of the samples showed a time-dependent increase in Fgd1 binding to cortactin upon TGF-β exposure (Fig. 6C). To explore this possibility further, the immunofluorescence experiment was repeated with cells which had been silenced for either Fgd1 or cortactin expression. The data presented in Fig. 6D and E show that, upon TGF-β treatment, cortactin localization remained unaltered in Fgd1-depleted cells, whereas Fgd1 translocation to the plasma membrane was impaired in the absence of cortactin. Collectively, these results show that TGF-β-induced Fgd1 recruitment to the subcortical skeleton involves cortactin.

An Fgd1 mutant with constitutively active exchange activity but impaired cortactin binding cannot induce podosome formation. Whereas TGF-β-induced podosomes assemble in ring-like structures (32), expression of V12Cdc42 triggers the formation of isolated podosomes scattered all over the ventral membrane of endothelial cells (20, 21). We therefore examined whether Fgd1 mutants known to exhibit constitutive activity toward Cdc42 could mimic these effects. Removing the N-terminal domain in a situation where the C-terminal portion of the molecule is truncated (25, 38) endows the mutated protein with constitutive activity toward Cdc42 in cell-free systems (37) as well as in cells (3, 25, 38). The myc-RKB3 fusion construct is deleted of residues 1 to 390 and thus lacks the N-terminal inhibitory GEF domain, the cortactin SH3 binding residues in the proline-rich domain, and the C-terminal portion of the molecule (Fig. 3) (25, 38). Myc-Fgd1-RKB3 expres-

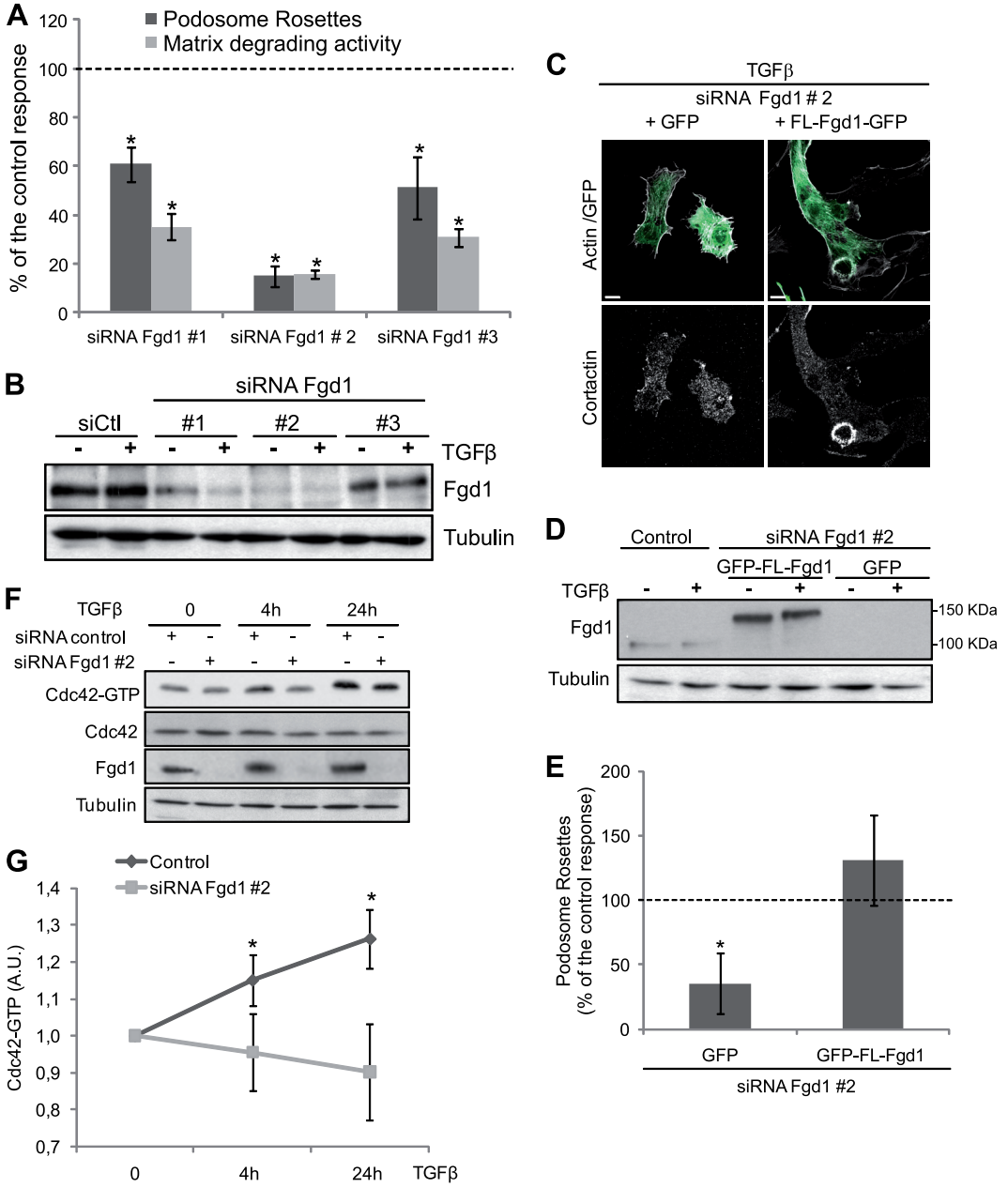

FIG. 5. Depletion of Fgd1 impairs TGF-β-induced podosome formation and Cdc42 activation. (A) Fgd1 was silenced in BAE cells using either of the three described siRNAs, and TGF-β stimulation was performed 24 h after the second siRNA transfection. For each condition, cells showing podosome rosettes were recorded and compared to the value obtained in the control siRNA condition, which was fixed arbitrarily at 100% for each experiment ($n = 4$). Alternatively, transfected cells were seeded on a gelatin-FITC matrix and stimulated with TGF-β for 24 h. Cells were fixed and double stained for F-actin and cortactin to record podosome-forming cells and assess matrix-degrading activities. The areas of gelatin degradation were quantified using ImageJ software, and the total degradation area was then normalized for the number of cells for each experiment ($n = 3$). (B) Western blot analysis of Fgd1 depletion in cells subjected to siRNA transfection used for the experiment described above. Similar tubulin levels seen in all lanes demonstrate equal protein loading. (C) BAE cells silenced for Fgd1 expression using siRNA#2 were transfected with a plasmid encoding GFP or GFP-FL-Fgd1 and stimulated for 24 h with TGF-β on the next day. (D) Western blot analysis of Fgd1 depletion and of Fgd1 reexpression using anti-GFP and anti-Fgd1 (Ab#1) antibodies in siRNA#2 silenced cells transfected with constructs encoding GFP-FL-Fgd1 or GFP alone in panel C showing effective depletion of the targeted proteins. (E) Quantification of cells showing podosome rosettes was performed in Fgd1 silenced BAE cells transfected with constructs encoding GFP-FL-Fgd1 or GFP alone, using GFP fluorescence. (F) The alterations of Cdc42 activities in BAE cells exposed to TGF-β for 4 or 24 h was assessed in pulldown assays using GST-CRIB-N-WASp fusion proteins, and the amounts of precipitated proteins were determined by Western blotting with specific antibodies. A fraction of whole-cell lysate was harvested and run in parallel to assess total Cdc42 protein contents. Similar tubulin levels in all lanes demonstrate equal protein loading. (G) Quantification of Cdc42 activation after scanning band intensities in the autoradiogram and processing of the data with NIH Image software ($n = 3$).

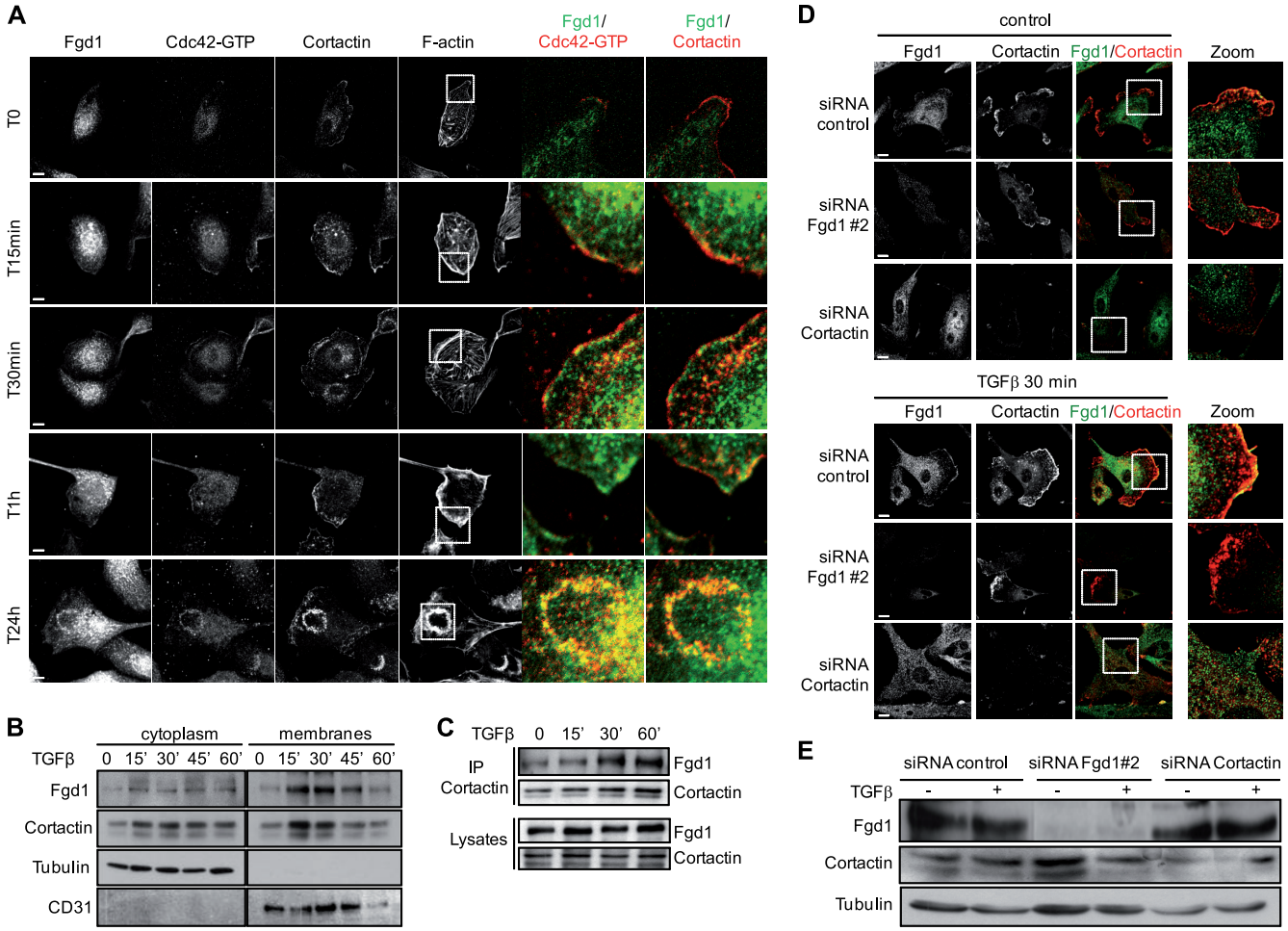

FIG. 6. Fgd1 and cortactin relocalize at the plasma membrane upon TGF-β stimulation. (A) Cells were treated with TGF-β for increasing time periods, fixed, and analyzed by immunofluorescence for Fgd1 (Ab#2), Cdc42-GTP, cortactin, and F-actin. Representative confocal images show individual staining for Fgd1, Cdc42-GTP, cortactin, and F-actin (bar, 10 μm). A magnified view of the boxed zone in the F-actin image shows the merge image of Fgd1 (green) and Cdc42 (red) or Fgd1 (green) and cortactin (red) stainings and their colocalization (yellow). (B) Western blot analysis of BAE cells extracts after cell fractionation, showing cytosolic and membrane/cytoskeleton-bound Fgd1 or cortactin in the course of TGF-β stimulation without serum. The purity of the extracts was assessed by reprobing the membrane for tubulin (cytoplasmic extracts) and CD31 (membrane extracts). (C) BAE cells were stimulated with TGF-β for increasing periods of time, and cortactin was immunoprecipitated. Samples were analyzed by Western blotting for cortactin and Fgd1 content (Ab#1). Similar Fgd1 and cortactin levels seen in all lanes corresponding to cell lysates demonstrate equal protein loading. (D) Same experiments as in panel A performed with cells which had been depleted of Fgd1 or cortactin by transfection of siRNA Fgd1 #2 or cortactin siRNA and subsequently stimulated with TGF-β for 30 min (bar, 10 μm). A magnified view of the boxed zone in the merge image shows details of Fgd1 and cortactin stainings (yellow) (bar, 10 μm). (E) Western blot analysis showing Fgd1 and cortactin expression in whole-cell lysates prepared from BAE cell cultures used in experiment depicted in panel D showing effective depletion of the targeted proteins.

sion did not stimulate the formation of podosome rosettes but induced the formation of isolated podosomes scattered all over the endothelial ventral membrane similarly to V12Cdc42 expression. In addition, the mutant was localized at these podosomes (Fig. 7A). We next examined the constitutively active mutant Fgd1-2DBDEL, which contains a larger portion of the PRD domain but lacks the PRD residues that negatively regulate exchange activity, the cortactin region, and the C-terminal portion of the molecule (2, 9) (Fig. 3). A significant fraction of GFP-Fgd1-2DBDEL localized at the plasma membrane (Fig. 7A), possibly by virtue of its PH domain or through a recently described mechanism involving serine 205 in the proline-rich domain (26). This indicated that some specific features of Fgd1 were retained in this mutant. However, it was unable to induce the formation of podosome rosettes or the assembly of isolated podosomes. Instead, GFP-Fgd1-2DBDEL expression induced the formation of disorganized peripheral F-actin clusters which contained podosomal markers such as cortactin, vinculin, P-Src, N-WASp, and Tks5 (Fig. 7B and data not shown). Since GFP-Fgd1-2DBDEL appeared to be capable of clustering major podosome components but unable to promote their proper organization in podosomal structures or superstructures, it appears that, in addition to promoting Cdc42-GDP exchange, other functions of Fgd1 are required for podosome rosette assembly. We therefore deleted the cortactin binding sequence (positions 156 to 165) to more specifically analyze the involvement of cortactin in Fgd1-mediated, TGF-β-induced, podosome rosette formation (Fig. 3). Cells

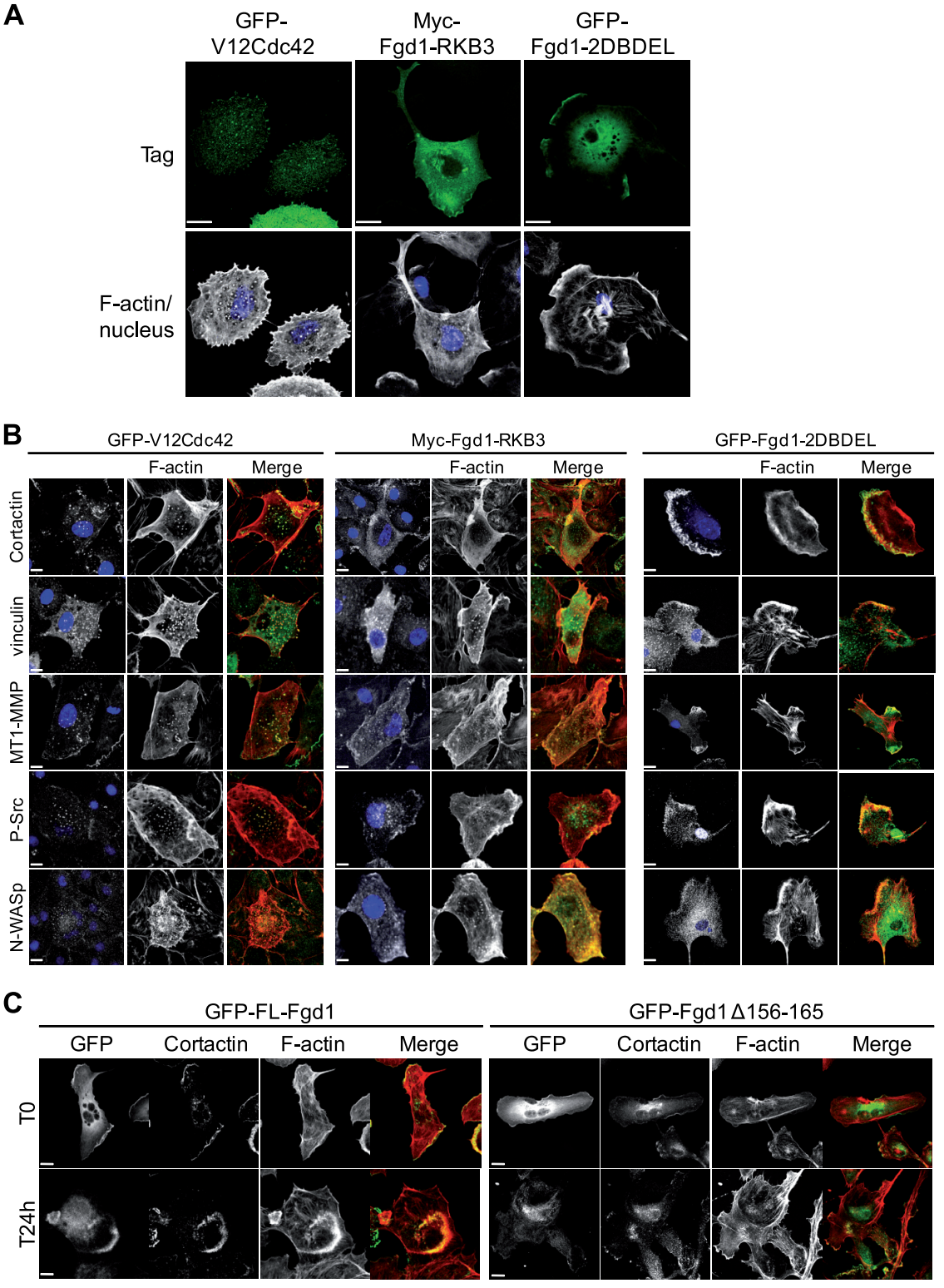

FIG. 7. Constitutively active Fgd1 fails to induce podosomes rosettes. (A) Representative confocal images of BAE cells transfected with a plasmid encoding either GFP-Cdc42, myc-Fgd1-RKB3, showing the localization of the tagged protein at podosomes, or GFP-Fgd1-2DBDEL showing that a fraction of the protein localizes at the plasma membrane. The corresponding staining for F-actin highlights the subcortical skeleton. Bar, 5 μm. (B) Representative images showing individual staining for cortactin, vinculin, MT1-MMP, P-Src, and N-WASp in BAE cells transfected with GFP-V12Cdc42, GFP-Fgd1-RKB3, or GFP Fgd1-2DBDEL, analyzed together with F-actin. Merged images of each protein (green) with F-actin (red) show accumulation of the protein at the subcortical skeleton; the nuclei are highlighted with Hoechst (blue) (bar, 10 μm). (C) Representative images showing individual staining for cortactin or F-actin in BAE cells transfected with GFP-FL-Fgd1 or GFP-Fgd1Δ156-165, analyzed together with F-actin. Merged images of each protein (green) with F-actin (red) show colocalization of the proteins in podosomes rosettes (GFP-Fgd1) or loosely assembled dots (GFP-Fgd1Δ156-165). The nuclei are highlighted with Hoechst strain (blue) (bar, 10 μm).

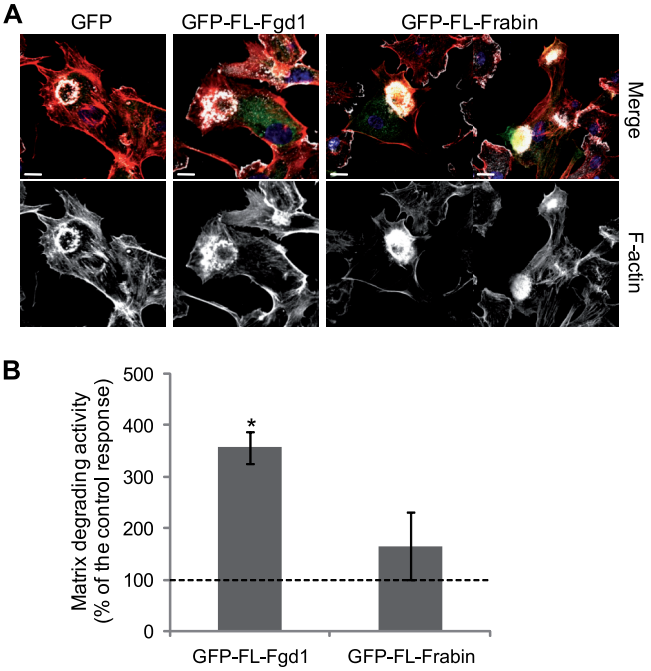

FIG. 8. Fgd1, but not Frabin, enhances BAE cell matrix-degrading activities. (A) Representative merged images of BAE cells transfected with GFP, GFP-FL-Fgd1, or GFP-Frabin encoding constructs, subsequently exposed to TGF-β for 24 h, stained for cortactin (white), F-actin (red), and nuclei (blue) are shown in the top panel (bar, 10 μm). Individual F-actin stainings in these images are shown in the bottom panel. (B) Same experiment as in panel A, performed with cells plated on a gelatin-FITC matrix and stained for cortactin and F-actin to record podosome-forming cells and assess matrix-degrading activities. The areas of gelatin degradation were quantified using ImageJ software. The total degradation area was then normalized for the number of cells for each experiment ($n = 3$) and is presented as a percentage of the control response measured in GFP-transfected cells arbitrarily taken as 100%.

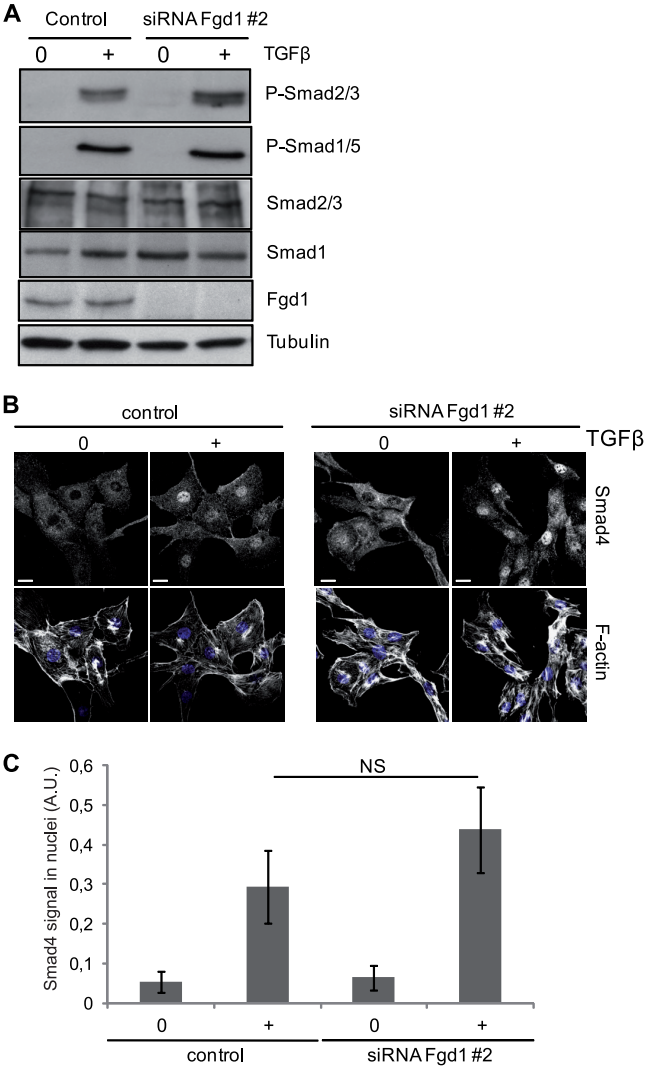

FIG. 9. Fgd1 regulates a novel noncanonical TGF-β pathway. Serum-starved BAE cells were stimulated with TGF-β for 30 min, and whole-cell lysates were examined for Smad1/5/8 and Smad2/3 phosphorylation by Western blotting. Similar Smad2/3 and Smad1 levels show no alteration in Smad expression. Depletion of Fgd1 was verified with Ab#1. Similar tubulin levels seen in all lanes demonstrate equal protein loading. (B) BAE cells were independently transfected with control siRNA or siRNAFgd1#2 and then left untreated or stimulated with TGF-β for 30 min. Representative confocal images of Smad4 and F-actin stainings are shown. (C) Smad4 nuclear signal was quantified on the basis of Hoechst staining using ImageJ software (50 cells for each condition) for each experiment ($n = 3$).

were transfected with GFP-Fgd1Δ156-165 or control GFP-Fgd1 and then stimulated with TGF-β. In TGF-β-treated cells, whereas GFP-Fgd1-expressing cells displayed typical podosome ring structures (40% versus GFP-transfected cells), the ability of cells transfected with Fgd1Δ1-165 to assemble rosettes was severely compromised (5% versus GFP-transfected cells). At best, cells formed loosely assembled dots, suggesting that some Fgd1 functions were still lacking (Fig. 7C). Since the GFP-Fgd1Δ156-165 is unable to support podosome formation, cortactin appears as an obligate Fgd1 partner in TGF-β signaling pathways in the process of podosome formation.

Fgd1 promotes matrix degradation. Frabin (Fgd4), another Cdc42-specific GEF with F-actin binding activity, was shown to enhance matrix degradation of invadopodia in RPMI7952 melanoma cells (22). We therefore compared the matrix-degrading activities of cells transfected with either GFP-Frabin or GFP-Fgd1 encoding constructs to that of cells transfected with a control GFP encoding plasmid. The percentage of cells displaying podosomes was found similar in cells expressing either construct. However, in contrast to cells expressing GFP-FL-Fgd1, cells expressing GFP-FL-Frabin exhibited disturbed ring organization, often showing larger rosettes filled with numerous podosomes (Fig. 8A), suggesting that Frabin interfered with podosome dynamics. However, in a gelatin degradation assay, overexpression of Fgd1, but not Frabin, stimulated a 2-fold increase in matrix degradation (Fig. 8B).

Fgd1 regulates a novel noncanonical TGF-β pathway. TGF-β-induced canonical Smad signaling has been well described in many cell types but the noncanonical pathways are less well understood and are likely to vary among cell types. In addition, some noncanonical pathways interfere with Smad phosphorylation. We therefore explored whether Fgd1 could affect Smad phosphorylation, which in these cells involves both Smad1/5 and Smad2/3 (32). The data presented in Fig. 9A show that

neither of these pathways was affected in Fgd1-depleted cells. Nuclear translocation of these complexes involves Smad4. To examine the possibility that Fgd1 could alter Smad translocation without affecting Smad phosphorylation, we examined Smad4 relocalization upon TGF-β stimulation in Fgd1-silenced cells. Figure 9B and C shows that Fgd1 depletion did not alter Smad4 relocalization in response to TGF-β treatment. These results suggest that Fgd1 is a key element of a novel noncanonical pathway downstream of the TGF-β receptor in aortic endothelial cells.

DISCUSSION

Podosome rosettes induced by TGF-β in aortic endothelial cells mediate matrix degradation events which could be involved in either basement membrane maintenance of large vessels or in the initiation of an invasive process (29). Here, we demonstrate a crucial role for Fgd1 in podosome formation and its importance in endothelial cell functions.

Fgd1 is an important actor in skeletal formation because mutations in this gene result in the disease faciogenital dysplasia or Aarskog-Scott syndrome (AAS), an X-linked developmental disorder that adversely affects the formation of multiple skeletal structures (27). Consequently, most studies have thus far focused on osteoblasts and osteoblast-like cell lines. Only recently, Fgd1 was shown to be expressed in certain tumor-derived cell lines and human tumors (3). By demonstrating Fgd1 expression in aortic endothelial cells, we establish here that Fgd1 is more widely expressed than initially thought in normal tissues. Furthermore, we show that Fgd1 might play an important role in vascular physiology and responses to inflammation. In support of this view, a human gene array technology study evaluating differences in gene expression in abdominal aortic aneurysm and arterial occlusive disease versus control aortic tissue revealed downregulation of Fgd1 gene expression in both diseases (1).

Fgd1 is the founding member of a family of highly related Fgd1-like genes. Fgd1 family members are modular proteins that contain in sequence an N-terminal domain, a Dbl homology (DH) domain, an adjacent pleckstrin homology (PH) domain, a FYVE-finger domain, and a second C-terminal PH domain (PH2). Each member contains a different N-terminal domain, suggesting interactions with distinct sets of regulatory molecules. The Fgd1 N-terminal domain contains a proline-rich region (PRD) involved in cortactin binding (16). In cultured primary mouse osteoblasts, Fgd1 was found in the cytosol, as well as in the Golgi and plasma membranes (10). In contrast, we found that in unstimulated BAE cells, the amount of Fgd1 at the subcortical actin cytoskeleton was low but increased upon TGF-β stimulation. We therefore anticipated that the activity of Fgd1 was turned on at an appropriate intracellular compartment through the interaction with upstream adaptor modules activated in a temporally and spatially regulated manner.

Our study shows that one such adaptor could be cortactin. Fgd1 is expected to regulate podosome formation through its exchange activity toward Cdc42, as supported by the consequences of Fgd1 knock down on TGF-β-induced Cdc42 activation. Indeed, the results obtained with the constitutively active Fgd1-RKB3 mutant show that this mutant behaves like V12Cdc42, suggesting that the large deletion in the PRD results in a loss of at least some of Fgd1 specificities. Constitutively active Fgd1-2DBDEL carrying a smaller deletion of the PRD but still lacking the cortactin binding domain retained some features of Fgd1, a fraction of the mutated protein localized at the cell cortex, possibly through a contribution of the PRD. However, this mutant failed to induce podosomes, indicating that, an as-yet-undefined membrane targeting function and/or the cortactin binding domain are critically involved in podosome formation. Moreover, unlike, FL-Fgd1, a mutant deleted of the sole cortactin binding region (Fgd1Δ156-165) was unable to support TGF-β-induced podosome formation. It therefore seems that Fgd1Δ156-165 cannot be recruited in TGF-β signaling pathways and competes with the endogenous molecule, thus preventing podosome assembly. Finally, TGF-β promoted Fgd1-cortactin association. Collectively, our results show that Fgd1 cortactin binding domain is essential for TGF-β-induced podosome formation.

The molecular association of Fgd1 and cortactin may be one aspect of the mechanism regulating the initial clustering of cortactin which act as nucleation platforms onto which the actin polymerization machinery assemble. Cortactin is composed of several protein interaction domains, an N-terminal acidic (NTA) region contains a conserved DDW region responsible for interaction with Arp3 and subsequent activation of the Arp2/3 complex, an F-actin binding region, a helical region, and a region rich in Pro, Ser, Thr, and Tyr that harbor sites of phosphorylation. Cortactin is therefore involved in subcellular regions engaged in *de novo* actin assembly, as typified by podosomes. Phosphorylation of cortactin by Src does not explain cortactin translocation at podosomes (39). Previous studies in vascular smooth muscle cells have shown that the SH3 domain of cortactin is required for cortactin clustering at the onset of podosome formation, while the actin binding repeat region is required for the translocation of cortactin to the actin-rich core of mature podosomes (39). These results suggest that the SH3 domain and the actin-binding repeat region are involved, respectively, in the early and late stages of podosome formation process (34). Fgd1 also binds Mabp1 (mammalian actin-binding protein 1) (16), a protein that structurally and functionally resembles cortactin (17) and which could therefore also contributes to rendering Fgd1 fully active. Although Mabp1 contains a helical, proline-rich, and SH3 domain at its carboxyl terminus, with sequence similarity with the cognate domains in cortactin, it does not contain an NTA domain or cortactin repeats. In our model, overexpression of FL-Fgd1 did not promote filopodia, a finding that is consistent with the fact that V12Cdc42 does not induce these structures in endothelial cells (21), nor did it promote podosome formation. It is likely that overexpression of Fgd1 leads to formation of unproductive Fgd1-cortactin (and Mabp1) complexes in the absence of concomitant Cdc42 activation. Our results provide the basis of a molecular mechanism involving Fgd1 and cortactin at the onset of podosome assembly. It is worth pointing out that Fgd1 has been shown is important for export from the Golgi bodies in some cells (9). Therefore, we cannot exclude that Fgd1 depletion also affects protein export from the Golgi bodies to the cell surface. However, the fact that the neoexpression of a plasmid encoding constitutively active Fgd1 mutant drives podosome formation supports our conclusions.

The induction of endothelial podosomes by TGF-β requires protein synthesis with a peak at 24 h after stimulation (32). At this stage, 20% of podosome rosettes stained for Fgd1, whereas cortactin was always present. This situation is similar to that found for invadopodia (3). The reasons for this are unclear, but it seems plausible that this observation reflects a dynamic turnover of Fgd1. One may envision that Fgd1 is recruited locally to initiate/drive actin polymerization and thus trigger podosome formation. Fgd1 then dissociates from this prepodosome and is recycled, thus becoming available for a new round of podosome rosette formation.

There is no published indication that Fgd1 may be tyrosine phosphorylated upon activation. Fgd1 protein domain organization, however, is similar to other GEFs already reported to be tyrosine kinase substrates. Also, putative phosphorylation sites in Fgd1 amino acid sequence point at Fgd1 as a plausible substrate for Src family kinases (data not shown). Finally, previous data obtained in this model show Src regulation upon exposure to TGF-β (32). Our data show that Fgd1 becomes tyrosine phosphorylated shortly after TGF-β addition, and this phosphorylation was found sensitive to Src family kinase inhibitors.

Considering these findings, we suggest a model whereby a signaling cascade triggered by TGF-β activates Fgd1. Activation is mediated by Src family kinases and promotes its association to binding partners, possibly cortactin (and/or Mabp1), to efficiently stimulate Cdc42 at the appropriate time and place. As far as cortactin is concerned, the mechanism may involve cortactin dimerization (18). Cdc42 in turn recruits the actin polymerization machinery, including actin related protein 2/3 complex (Arp2/3) and neuronal Wiskott-Aldrich syndrome protein (N-WASp), leading to actin polymerization at the core of the podosome and subsequent recruitment of adhesion proteins.

Our previous studies established that Smad signaling is required for TGF-β-induced podosome assembly. The present study brings evidence for the contribution of a parallel signaling pathway leading to Cdc42 activation, in the process of podosome formation. The description of this novel noncanonical pathway may also shed light on mechanisms such as ossification and skeletal development, where Fgd1 signaling plays a critical role. Because TGF-β is an important regulator of bone biogenesis, it is tempting to speculate that the defects observed in faciogenital dysplasia may result, at least in part, from altered TGF-β signaling. Likewise, our findings predict a perturbation in the vascular system in AAS. In this respect, arterial dysplasia, malformation, and aneurysms have recently been reported in this disease (7). It is thus likely that future studies will further elucidate the involvement of Fgd1 in vascular diseases.

The present findings contribute to our understanding of the basic mechanisms of podosome formation and function, by shedding light on the mechanism by which Fgd1 in combination with cortactin mediates the clustering of podosome components and initiate actin polymerization which gives rise to podosomal structures. They not only clarify a novel mechanism for podosome formation but also provide clues to understanding the role of podosomes in TGF-β-enriched tissue environments. For the first time, Fgd1 emerges as an important regulator in the vascular system. These studies also establish that Fgd1 is a regulatory element of signaling cascades triggered by TGF-β and thereby provide the basis of a novel noncanonical pathway. Such pathway is involved in the process of podosome formation but could also contribute to other TGF-β-mediated processes in cell physiology and pathology.

ACKNOWLEDGMENTS

Funding for this research was provided by ANR 2010 BLAN 1237 01, ARC 5040, and CNRS GDR 2823 to E.G., by the Italian Association for Cancer Research to R.B., and by the European Union's Seventh Framework Programme (FP7/2007-2013) to E.G. and R.B. under grant agreement 237946. T.D. is the recipient of a fellowship from Association pour la Recherche sur le Cancer.

We thank R. Garcia-Mata and K. Burridge (University of North Carolina at Chapel Hill) for providing the Cdc4215A construct, J. L. Gorski (University of Michigan) for all Fgd1 constructs, and A. Hall (Sloan-Kettering Cancer Center, New York, NY) for providing myc-Fgd1-RKB3. The plasmid encoding GFP-Frabin was kindly provided by Yoshimi Takai (Kobe University, Kobe, Japan), and anti-Zizimin antibodies were kindly provided by M. Schwartz (University of Virginia at Charlottesville). We thank Ijsbrand Kramer for critical reading of the manuscript.

REFERENCES

1. **Armstrong, P. J., et al.** 2002. Differential gene expression in human abdominal aorta: aneurysmal versus occlusive disease. J. Vasc. Surg. **35:**346–355.
2. **Ayala, I., et al.** 2008. Multiple regulatory inputs converge on cortactin to control invadopodia biogenesis and extracellular matrix degradation. J. Cell Sci. **121:**369–378.
3. **Ayala, I., et al.** 2009. Faciogenital dysplasia protein Fgd1 regulates invadopodia biogenesis and extracellular matrix degradation and is upregulated in prostate and breast cancer. Cancer Res. **69:**747–752.
4. **Brantley-Sieders, D. M., et al.** 2009. Host deficiency in Vav2/3 guanine nucleotide exchange factors impairs tumor growth, survival, and angiogenesis in vivo. Mol. Cancer Res. **7:**615–623.
5. **Brown, K. A., et al.** 2008. Identification of novel Smad2 and Smad3 associated proteins in response to TGF-β1. J. Cell Biochem. **105:**596–611.
6. **Buccione, R., J. D. Orth, and M. A. McNiven.** 2004. Foot and mouth: podosomes, invadopodia and circular dorsal ruffles. Nat. Rev. Mol. Cell. Biol. **5:**647–657.
7. **Diluna, M. L., N. M. Amankulor, M. H. Johnson, and M. Gunel.** 2007. Cerebrovascular disease associated with Aarskog-Scott syndrome. Neuroradiology **49:**457–461.
8. **Dubash, A. D., et al.** 2007. A novel role for Lsc/p115 RhoGEF and LARG in regulating RhoA activity downstream of adhesion to fibronectin. J. Cell Sci. **120:**3989–3998.
9. **Egorov, M. V., et al.** 2009. Faciogenital dysplasia protein (FGD1) regulates export of cargo proteins from the Golgi complex via Cdc42 activation. Mol. Biol. Cell **20:**2413–2427.
10. **Estrada, L., E. Caron, and J. L. Gorski.** 2001. Fgd1, the Cdc42 guanine nucleotide exchange factor responsible for faciogenital dysplasia, is localized to the subcortical actin cytoskeleton and Golgi membrane. Hum. Mol. Genet. **10:**485–495.
11. **Feng, Q., D. Baird, S. Yoo, M. Antonyak, and R. A. Cerione.** 2010. Phosphorylation of the cool-1/β-Pix protein serves as a regulatory signal for the migration and invasive activity of Src-transformed cells. J. Biol. Chem. **285:**18806–18816.
12. **Furmaniak-Kazmierczak, E., S. W. Crawley, R. L. Carter, D. H. Maurice, and G. P. Cote.** 2007. Formation of extracellular matrix-digesting invadopodia by primary aortic smooth muscle cells. Circ. Res. **100:**1328–1336.
13. **Garcia-Mata, R., et al.** 2007. The nuclear RhoA exchange factor Net1 interacts with proteins of the Dlg family, affects their localization, and influences their tumor suppressor activity. Mol. Cell. Biol. **27:**8683–8697.
14. **Gimona, M., R. Buccione, S. A. Courtneidge, and S. Linder.** 2008. Assembly and biological role of podosomes and invadopodia. Curr. Opin. Cell Biol. **20:**235–241.
15. **Goumans, M. J., and C. Mummery.** 2000. Functional analysis of the TGFβ receptor/Smad pathway through gene ablation in mice. Int. J. Dev. Biol. **44:**253–265.
16. **Hou, P., et al.** 2003. Fgd1, the Cdc42 GEF responsible for faciogenital dysplasia, directly interacts with cortactin and Mabp1 to modulate cell shape. Hum. Mol. Genet. **12:**1981–1993.
17. **Kessels, M. M., A. E. Engqvist-Goldstein, and D. G. Drubin.** 2000. Association of mouse actin-binding protein 1 (Mabp1/SH3P7), an Src kinase target, with dynamic regions of the cortical actin cytoskeleton in response to Rac1 activation. Mol. Biol. Cell **11:**393–412.
18. **Kim, K., P. Hou, J. L. Gorski, and J. A. Cooper.** 2004. Effect of Fgd1 on

cortactin in Arp2/3 complex-mediated actin assembly. Biochemistry **43:**2422–2427.
19. **Linder, S., and M. Aepfelbacher.** 2003. Podosomes: adhesion hot-spots of invasive cells. Trends Cell Biol. **13:**376–385.
20. **Moreau, V., et al.** 2006. Cdc42-driven podosome formation in endothelial cells. Eur. J. Cell Biol. **85:**319–325.
21. **Moreau, V., F. Tatin, C. Varon, and E. Genot.** 2003. Actin can reorganize into podosomes in aortic endothelial cells, a process controlled by Cdc42 and RhoA. Mol. Cell. Biol. **23:**6809–6822.
22. **Nakahara, H., et al.** 2003. Involvement of Cdc42 and Rac small G proteins in invadopodia formation of RPMI7951 cells. Genes Cells **8:**1019–1027.
23. **Nakanishi, H., and Y. Takai.** 2008. Frabin and other related Cdc42-specific guanine nucleotide exchange factors couple the actin cytoskeleton with the plasma membrane. J. Cell Mol. Med. **12:**1169–1176.
24. **Nobes, C. D., and A. Hall.** 1995. Rho, rac, and cdc42 GTPases regulate the assembly of multimolecular focal complexes associated with actin stress fibers, lamellipodia, and filopodia. Cell **81:**53–62.
25. **Olson, M. F., N. G. Pasteris, J. L. Gorski, and A. Hall.** 1996. Faciogenital dysplasia protein (FGD1) and Vav, two related proteins required for normal embryonic development, are upstream regulators of Rho GTPases. Curr. Biol. **6:**1628–1633.
26. **Oshima, T., T. Fujino, K. Ando, and M. Hayakawa.** 2010. Proline-rich domain plays a crucial role in extracellular stimuli-responsive translocation of a Cdc42 guanine nucleotide exchange factor, FGD1. Biol. Pharm. Bull. **33:**35–39.
27. **Pasteris, N. G., et al.** 1995. Cloning and regional localization of the mouse faciogenital dysplasia (Fgd1) gene. Mamm. Genome. **6:**658–661.
28. **Rottiers, P., et al.** 2009. TGFbeta-induced endothelial podosomes mediate basement membrane collagen degradation in arterial vessels. J. Cell Sci. **122:**4311–4318.
29. **Saltel, F., et al.** 2011. Invadosomes: intriguing structures with promise. Eur. J. Cell Biol. **90:**100–107.
30. **Schmidt, S., S. Diriong, J. Mery, E. Fabbrizio, and A. Debant.** 2002. Identification of the first Rho-GEF inhibitor, TRIPα, which targets the RhoA-specific GEF domain of Trio. FEBS Lett. **523:**35–42.
31. **Tatin, F., C. Varon, E. Genot, and V. Moreau.** 2006. A signaling cascade involving PKC, Src and Cdc42 regulates podosome assembly in cultured endothelial cells in response to phorbol ester. J. Cell Sci. **119:**769–781.
32. **Varon, C., et al.** 2006. Transforming growth factor beta induces rosettes of podosomes in primary aortic endothelial cells. Mol. Cell. Biol. **26:**3582–3594.
33. **Webb, B. A., et al.** 2005. PAK1 induces podosome formation in A7r5 vascular smooth muscle cells in a PAK-interacting exchange factor-dependent manner. Am. J. Physiol. Cell Physiol. **289:**C898–C907.
34. **Webb, B. A., R. Eves, and A. S. Mak.** 2006. Cortactin regulates podosome formation: roles of the protein interaction domains. Exp. Cell Res. **312:**760–769.
35. **Xu, M., et al.** 2010. Familial syndrome resembling Aarskog syndrome. Am. J. Med. Genet. A **152A:**2017–2022.
36. **Zhang, Y., et al.** 2007. Regulation of ephexin1, a guanine nucleotide exchange factor of Rho family GTPases, by fibroblast growth factor receptor-mediated tyrosine phosphorylation. J. Biol. Chem. **282:**31103–31112.
37. **Zheng, Y., et al.** 1996. The faciogenital dysplasia gene product FGD1 functions as a Cdc42Hs-specific guanine-nucleotide exchange factor. J. Biol. Chem. **271:**33169–33172.
38. **Zhou, K., et al.** 1998. Guanine nucleotide exchange factors regulate specificity of downstream signaling from Rac and Cdc42. J. Biol. Chem. **273:**16782–16786.
39. **Zhou, S., B. A. Webb, R. Eves, and A. S. Mak.** 2006. Effects of tyrosine phosphorylation of cortactin on podosome formation in A7r5 vascular smooth muscle cells. Am. J. Physiol. Cell Physiol. **290:**C463–C471.